

Full Paper

Ampicillin as a Potential Environmentally Friendly Corrosion Inhibitor for 60Cu-40Zn Brass in Nitric Acid Medium: Experimental and Computational Investigations

Sofiane Sebiane,¹ Farida Kellou-Kerkouche,¹ and Brahim Idir^{1,2,*}

¹*USTHB, Laboratory of Electrochemical-Corrosion, Metallurgy and Mineral Chemistry BP32 El-Alia Bab-Ezzouar, 16111, Algiers, Algeria*

²*Research Center in Industrial Technologies (CRTI), P.O. Box 64, Cheraga 16014 Algiers, Algeria*

*Corresponding Author, Tel.: +213550737152

E-Mail: idirbrahim2016@gmail.com

Received: 12 April 2023 / Received in revised form: 30 September 2023 /

Accepted: 10 October 2023 / Published online: 31 October 2023

Abstract- In the current study, outdated Ampicillin drug (AMP) was assessed as a potent and environmentally friendly corrosion inhibitor for 60Cu-40Zn brass by gravimetric analysis, in nitric acid solution in a concentration range of 0.5M-2M. The findings revealed that AMP exhibited high corrosion inhibition performance, and its efficiency increased with the increase of its concentration and the concentration of nitric acid. In addition, potentiodynamic polarization (PDP) curves, electrochemical impedance spectroscopy (EIS), and surface analysis were conducted in 0.5 M HNO₃ solution. Ampicillin was found to act as a mixed-type inhibitor, and its inhibitory efficiency increased with the addition of AMP up to 92% at its optimal concentration of 10 mM. However, it decreased slightly with increasing temperature. The adsorption thermodynamic parameters demonstrated that the medicine adsorbed onto a brass surface in accordance with the Langmuir isotherm, via physisorption and chemisorption mechanism. Scanning Electron Microscopy (SEM), Energy Dispersive X-ray (EDX) and FT-IR/ATR analysis clearly evidenced the strong adsorption of AMP onto the brass surface, leading to higher corrosion resistance of the brass alloy in the inhibitive solution. Theoretical parameters of drug molecules were computed, using density functional theory (DFT) and Fukui indices, to better understand the adsorption mechanism of AMP molecules onto the brass surface. A close agreement between quantum calculations and experimental results was observed.

Keywords- Brass corrosion; Nitric acid; Corrosion inhibition; Electrochemical methods; Quantum parameters

1. INTRODUCTION

Brass materials are highly ductile and malleable mainly composed of copper and zinc and are the most popular copper alloys depending on their field of application [1]. They have excellent electrical and thermal conductivity making them excellent candidates for a wide range of applications, including heating and air conditioning systems, high-tech industry, manufacture of fittings, valves, tanks, impellers, musical instruments, etc. They are also used in oil refineries, chemical plants, and marine engineering [2-5]. Their pleasing color, excellent formability, and drawing characteristics make them indispensable for the manufacture of jewelry, statues, and other decorative items [3]. Increasing zinc content of the alloy followed by appropriate thermo-mechanical treatment, has led to the development of a wide variety of Cu-Zn alloys with good physical and mechanical properties [6]. This kind of alloy is susceptible to corrosion and its dissolution process is greatly accelerated as the zinc content increases. This phenomenon is known as dezincification, which is considered to be a major factor limiting the use of brass in many applications [1,7-8]. Therefore, alloys Cu-Zn (70/30) and (60/40) are very sensitive to corrosion, while alloy (85/15) is much less so. It is worth noting that among corrosive environments, nitric acid is identified as a powerful oxidizing agent that can easily corrode copper and its alloys [9]. The brass surface being chemical, physical, and energetically heterogeneous, it can be considered as another reason why the corrosive process operates easily [10]. However, the extent of this phenomenon depends on both the nature of the corrosive environment and the type of cathodic process [11]. The use of corrosion inhibitors is one of the many practical and effective methods to reduce the dissolution of metallic alloys in aggressive acidic environments [12-16]. Nowadays, organic molecules that contain nitrogen, sulfur, oxygen, and aromatic rings are promoted. However, their effectiveness mainly depends on their ability to adhere to the metal surface [17-19]. The efficiency of the inhibitor depends on various parameters, including the nature of the metal surface, the environment, the electrochemical potential of the interface, and the structure of the inhibitor. This latter includes the number of adsorption centers in the molecule, their charge density, molecular size, and adsorption mode. Usually, acid pickling operates at elevated temperatures [20] and in spite of these favoring parameters, the efficiency of many organic inhibitors decreases as the temperature rises. Therefore, it is important to find an inhibitor that maintains its properties even at high temperatures. Chemisorption has been reported to be responsible for retaining the inhibition efficiency at high temperatures [21]. The development and use of corrosion inhibitors have been continuously gaining momentum in recent years. Unfortunately, the most effective corrosion inhibitors that have been used for decades are toxic. For this reason, current scientific research focuses on the development of eco-friendly inhibitors [22,23]. The employment of non-toxic inhibitors has become the main requirement in the industry [24]. Therefore, in recent years, researchers have developed alternative eco-friendly corrosion inhibitors, including rare earth elements [25], amino acids [20,26], essential

oils of extract plants [27], and drugs [28,29]. This class of inhibitors has gained a lot of interest from a large number of scientists. Some medicines exhibit exceptional effects on preventing the corrosion of various alloys in aggressive environments. Indeed, good inhibition efficiency has been obtained by using Rhodanine Azosulpha [30] and anti-bacterial drugs [31] that hinder the corrosion of stainless steel in hydrochloric acid electrolytes. Some antibiotic drugs [32-34] acted as inhibitors to enhance the corrosion resistance of aluminum in HCl, whereas antihypertensive drugs [35] have enhanced the corrosion performance of aluminum alloys in aqueous solutions. Different anti-fungal and anti-inflammatory drugs [36,37] were tested as corrosion inhibitors for metals in various environments. Regarding copper, its corrosion resistance in NaCl was improved by adding an antiemetic drug in the corrosive solution [38]. Recently, a list of different classes of drugs was edited as corrosion inhibitors for different alloys [39].

The Ampicillin drug was chosen as a corrosion inhibitor in this investigation based on the following parameters: non-toxicity, relatively low cost, and a molecular structure which has several functional groups such as $-NH_2$; $-C=O$; $-COOH$, an aromatic ring, as well as heteroatoms like O, N, and specifically sulfur atom, which can cause greater adsorption on the surface of the brass.

The present work was initiated to evaluate the inhibitory capacity of expired Ampicillin (AMP) as a corrosion inhibitor for brass (60Cu-40Zn) in 0.5, 1, 1.5, and 2 M nitric acid solutions, using the gravimetric method combined with SEM, EDX, and FT-IR/ATR analysis to characterize the adsorbed film on the brass surface.

Electrochemical techniques such as PDP and EIS were used to predict the electrochemical corrosion behavior of brass with and without the addition of the inhibitor in 0.5 M HNO_3 solution. Finally, to better understand the corrosion inhibition mechanism and the donor-acceptor relationship between the inhibitor molecules and the brass surface, the theoretical parameters of AMP molecule and its protonated form were computed using density functional theory (DFT) in the water phase.

2. EXPERIMENTAL SECTION

2.1. Material preparation

The commercial brass studied has the following chemical composition by (weight%): 59.5% Cu, 0.25% Sn, 0.15% Fe, 0.45% Pb, and balance Zn. The working electrode used for electrochemical tests was a round rod that was mechanically cut. It was connected to a copper wire and embedded with epoxy resin, providing an active surface area of 0.196 cm^2 . Before each electrochemical test, the electrode is abraded using Silicon Carbide papers (ranging from 600 to 1200 grade). It is then rinsed with bi-distilled water and degreased with acetone right before being introduced into the electrochemical cell.

2.2. Aggressive and inhibitive solutions

Aggressive HNO₃ solutions (0.5, 1, 1.5, and 2 M) were prepared by diluting of analytical reagent grade, 69% HNO₃ (Sigma Aldrich Chemicals) with distilled water. Four Ampicillin drug concentrations of 0.5, 1, 5, and 10 mM were used to evaluate its corrosion-inhibiting power for brass in 0.5M nitric acid medium.

Ampicillin belongs to a class of medications called penicillin's and the chemical molecular structure of this compound is shown in Figure 1.

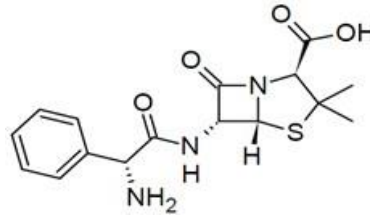


Figure 1. Chemical molecular structure of AMP

2.3. Gravimetric (weight loss) method

In the gravimetric experiment, a polished brass coupon that had been weighed beforehand was fully submerged in 150 mL of the test solution in an uncovered beaker. The latter was placed in a water bath that was kept at a constant temperature. After 6 hours, the coupons were taken out. Each coupon was dipped in acetone and left to dry in the air before being weighed again. The change in weight was considered as the total weight loss. The experiments were repeated with varying inhibitor and nitric acid concentrations. Based on the weight loss results, the inhibition efficiency (IE%), degree of surface coverage (θ), and corrosion rates (CR) were calculated using Equations (1), (2), and (3) respectively.

$$IE\% = \left(1 - \frac{W_1}{W_2}\right) \times 100 \quad (1)$$

$$\theta = 1 - \frac{W_1}{W_2} \quad (2)$$

$$CR \text{ (mg cm}^{-2} \text{ h}^{-1}\text{)} = \frac{W}{A t} \quad (3)$$

The weight losses (mg) for brass in the presence and absence of the inhibitor in the HNO₃ solution are represented by W_1 and W_2 , respectively. The degree of surface coverage of the inhibitor is represented by θ . A represents the area of the brass coupon in cm², t represents the period of immersion in hours, and W represents the weight loss of brass after time t . All measurements were performed three times, and the average value was recorded.

2.4. Electrochemical methods

EIS technique provides detailed information about the resistive and capacitive behavior of the electrified interface, to assess the corrosion of brass in a 0.5 M HNO₃ solution, with and

without AMP. Experiments were conducted at the open circuit potential, after a 30 min stabilization period, over a frequency range of 100 kHz to 10 mHz, with a 10-mV peak-to-peak voltage excitation, by using a Potentiostat-Galvanostat (Princeton Applied Research Versastat 3) controlled by a computer using Versa-studio software. Potentiodynamic polarization curves were obtained using a conventional three-electrode cell. The saturated calomel electrode (SCE) was used as the reference electrode (RE), and a platinum foil with a surface area of 1.0 cm² was used as the counter electrode. The brass sample, which has an active surface area of 0.196 cm², was used as the working electrode (WE). The curves were plotted from -300 mV to +300 mV relative to the open circuit potential (OCP), at a scan rate of 1 mV/s.

The inhibition efficiency (IE %) from EIS and the polarization curves were calculated by the equations (4) and (5), respectively:

$$IE\% = \frac{R_1 - R_{1,0}}{R_1} \times 100 \quad (4)$$

$$IE\% = \frac{i_{cor,0} - i_{cor}}{i_{cor,0}} \times 100 \quad (5)$$

Here: i_{cor} and $i_{cor,0}$ represent corrosion current density with and without inhibitor, respectively. R_1 and $R_{1,0}$ represent charge transfer resistance with and without inhibitors, respectively.

The surface coverage has been also calculated, with equations (6 and 7), using Tafel and EIS parameters, respectively:

$$\theta = \frac{i_{cor,0} - i_{cor}}{i_{cor,0}} \quad (6)$$

$$\theta = \frac{R_1 - R_{1,0}}{R_1} \quad (7)$$

2.5. Characterization and analysis studies

In view of determining the phases present in the microstructure of 60Cu-40Zn brass, the sample was chemically etched with iron chloride solution for a few seconds, then removed, washed with bi-distilled water, and properly dried. An optical microscope (Nikon Eclipse LV100ND) has been employed to examine the brass surface. The optical micrograph of the etched surface is provided in Figure 2. Two phases are well visible, one light is rich in Cu, this is the (α) phase, and the other is dark and rich in Zn, it is called the (β') phase.

To observe and analyze the surface of the brass, it was immersed in a 0.5 M HNO₃ solution for 6 hours. This was done both with and without AMP at its optimal concentration. Before immersing the brass, it was mechanically treated by abrading it with emery papers to achieve a smooth surface, rinsing it with double distilled water, and then degreasing it with acetone. After the immersion of the cleaned specimen, in the test solutions, it was removed, cleaned with bi-distilled water, and dried with a cold air stream, and then its surface morphologies were characterized using scanning electron microscopy SEM (Zeiss Gemini300), coupled with energy dispersive X-ray analyzer EDX (Zeiss Gemini300), at accelerating voltage of 20 kV.

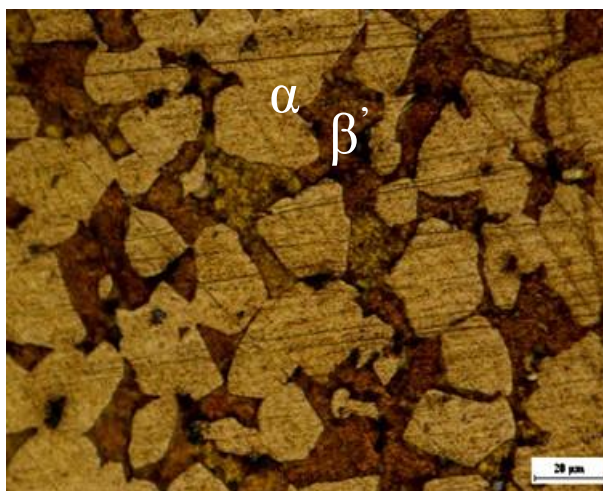


Figure 2. Optical micrograph of the etched brass

2.6. Spectroscopic study (FT-IR)

FT-IR spectra, of pure Ampicillin (AMP) and of scraped layer recovered from 60Cu-40Zn alloy were recorded using a Shimadzu FTIR 8000 type in the scanning range of 4000-400 cm^{-1} . The brass sample was immersed in the 0.5 M HNO_3 acid solution containing 10 mM of AMP for 6 hours. Then the sample was taken, washed with distilled water, and dried. The inhibitor film adsorbed on the specimen surface was delicately scraped off and collected [40]. The pure AMP and the collected AMP/60Cu-40Zn film were mixed and compacted with potassium bromide KBr to pellets form, and then their FT-IR spectra were recorded.

2.7. Theoretical calculations

The computational calculations were determined using the Spartan 08 program package [36]. Full geometry optimization of the molecule was obtained using the DFT method at the basis set B3LYP/6-31G (d, p) level of theory, in a water phase. Several quantum descriptors, including the energy of the highest occupied molecular orbital (E_{HOMO}), energy of the lowest unoccupied molecular orbital (E_{LUMO}), and dipole moment (μ), have been determined. The absolute electronegativity (χ) and hardness (η) were obtained by means of the equations (8) and (9) [41]:

$$\chi = \frac{I+A}{2} \quad (8)$$

$$\eta = \frac{I-A}{2} \quad (9)$$

The ionization potential, denoted as $I = -E_{\text{HOMO}}$, and the electron affinity, denoted as $A = -E_{\text{LUMO}}$.

Global electrophilicity index (ω) and nucleophilicity (ϵ), which is equal to $(1/\omega)$, are deduced from the following equations:

$$\omega = \frac{\chi^2}{2\eta} \quad (10)$$

$$\varepsilon = \frac{1}{\omega} = \frac{2\eta}{\chi^2} \quad (11)$$

To better understand the reactivity of the AMP molecule, we determined the Fukui indices (Eqs.12 and 13) by approximating the finite difference from the Mulliken population analysis (MPA) of atoms for AMP and protonated AMP:

$$f_k^+ = q_k(N + 1) - q_k(N) \quad (12)$$

$$f_k^- = q_k(N) - q_k(N - 1) \quad (13)$$

where $q_k(N)$, $q_k(N + 1)$ and $q_k(N - 1)$ are the atomic charges of the systems with N, N+1, and N-1 electrons, respectively.

3. RESULTS AND DISCUSSION

3.1. Weight loss measurements

The gravimetric method is often used to determine the corrosion rate because it is simple to apply and accurate [42]. Table 1 illustrates the calculated values of corrosion rate (*CR*) of brass electrode, immersed for 6 hours at 25°C, and inhibitory effectiveness (*IE*%) as a function of drug concentrations at various concentrations of nitric acid. It is clear that the *CR* decreases as the AMP concentration increases, and as a result, the *IE* percentage increases with the addition of the drug. This result proves the effectiveness of expired AMP on the corrosion of brass in all acid solutions.

The results clearly show that regardless of the acid concentration, the corrosion rate (*CR*) decreases when expired AMP is present, and increases as the acid concentration increases when the drug is not present. This suggests that Ampicillin in the acid solution prevents brass corrosion in HNO₃, and the extent of corrosion prevention depends on the amount of Ampicillin present. In fact, the corrosion inhibition efficiency of AMP reached its highest value of 95.36% in the most acidic solution (2 M HNO₃) at the optimal drug concentration (10 mM). We also observed that the inhibition efficiency increased as the concentration of AMP increased.

It is well known that the oxidizing power of nitric acid depends on its concentration [13]. For obtaining more information on the corrosion inhibition of AMP, the effect of various nitric acid concentrations on the corrosion rate (*CR*) without and with the various additions of AMP, obtained from the weight loss method, were determined by the expression proposed by Mathur and Vasudevan [43]:

$$\ln CR = \ln K + BC \quad (14)$$

K is the rate constant, *B* is the reaction constant and *C* is the molar concentration of HNO₃. According to Eq (14), *K* may be defined as a starting rate at zero acid concentration, so it informs us about the corrosivity of acid towards the metal [43]. *B* is the slope of the straight

line of $\ln CR$ vs C [44]. The straight lines obtained of $\ln CR$ vs C in uninhibited and inhibited acid solutions (not shown here), suggest that the kinetic equation proposed by Mathur and Vasudevan is applicable and valid [45,46]. In the studied experimental tests, the values of K and B obtained in the absence and presence of AMP drug were 2.12, 1.25, 0.74, 0.44, 0.24 ($\text{mg cm}^{-2} \text{h}^{-1}$) and 1.02, 0.73, 0.69, 0.54, 0.57 ($\text{mg cm}^{-2} \text{h}^{-1} \text{M}^{-1}$), respectively. The higher value of K in the blank HNO_3 solution compared to that in the inhibited HNO_3 solutions suggests that the HNO_3 solution has a greater ability to corrode brass and that this aggressiveness increases with increasing acid concentration from 0.5 to 2 M. Similar variations of kinetic parameters (K and B) were reported by X. Wang et al [44].

Table 1. Gravimetric measurements of brass in various concentrations of HNO_3 solution without and with inhibitor concentrations at 25°C

[HNO_3]	[AMP] (mM)	CR ($\text{mg cm}^{-2} \text{h}^{-1}$)	IE (%)	θ
0.5 M	0	3.07	/	/
	0.5	1.59	48.22	0.4822
	1	0.91	70.35	0.7035
	5	0.51	83.29	0.8329
	10	0.27	91.17	0.9117
1 M	0	7.17	/	/
	0.5	3.15	56.06	0.5606
	1	1.81	74.70	0.7470
	5	0.89	87.52	0.8752
	10	0.54	92.46	0.9246
1.5 M	0	9.48	/	/
	0.5	3.71	60.83	0.6083
	1	2.16	77.24	0.7724
	5	1.04	89.07	0.8907
	10	0.58	93.90	0.9390
2 M	0	14.87	/	/
	0.5	5.07	65.89	0.6589
	1	2.71	81.75	0.8175
	5	1.21	91.84	0.9184
	10	0.69	95.36	0.9536

We can notice that the values of K and B decreased in the presence of AMP in the acid solution. These results indicate that AMP inhibitor slowed down the dissolution process of brass. Moreover, for the same AMP concentration, the inhibition efficiency increased with increasing of acid concentration which implies that AMP is an excellent brass inhibitor in nitric acid medium, even at high acid concentration [44].

3.2. Electrochemical study

To carry out the electrochemical study of the AMP corrosion inhibitory effect, we retained the concentration of 0.5 M for the corrosive tested solution.

3.2.1. Potentiodynamic polarization results

The polarization curves of brass in 0.5 M HNO₃ solution at 25°C are shown in Figure 3, both with and without various amounts of AMP. Table 2 gathers the different electrochemical kinetic parameters obtained by extrapolating the two Tafel linear to the corrosion potential.

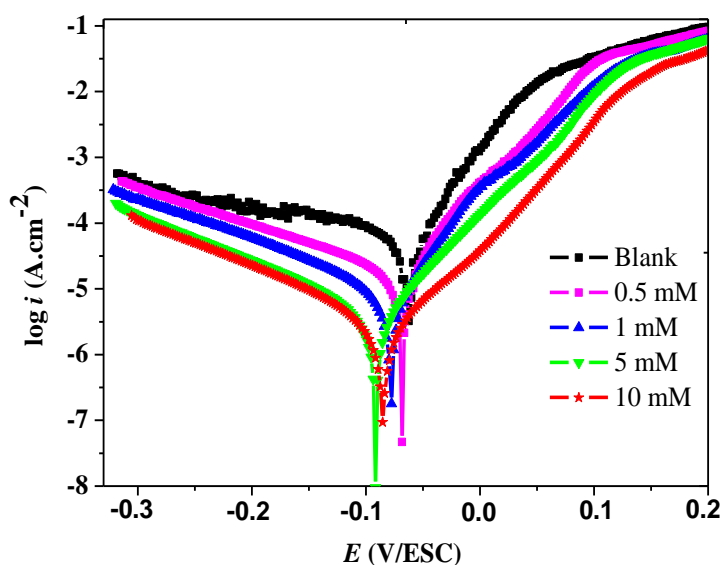


Figure 3. Potentiodynamic polarization curves of brass in 0.5 M HNO₃ containing different concentrations of AMP at 25 °C with a scan rate of 1 mV/s

Figure 3 shows that as the amounts of AMP increase in acidic solution, the anodic and cathodic current densities decrease. However, the overall shape of the curve remains the same, indicating that the reduction and oxidation mechanisms are unchanged.

Table 2 revealed that the increase of the AMP concentration induced a significant decrease of the corrosion current densities (i_{cor}). This can be explained by the improvement of the corrosion resistance of the brass sample [47]. The values of the two Tafel slopes (ba and bc) have similar magnitudes in the blank and inhibitive solutions, indicating that the corrosion mechanism of the brass is unaltered by the presence of AMP. Moreover, the corrosion potential (E_{cor}) remains relatively unchanged, suggesting that the drug is adsorbed on both the anodic and cathodic sites of the metal surface. Therefore, it can be concluded that AMP acts as a mixed-type inhibitor [48]. The inhibition efficiency ($IE\%$) increases up to 92% when the AMP concentration reaches the optimum value of 10 mM. This suggests that the protective adsorption film, on the brass surface, becomes complete and more stable [49].

Table 2. Effect of AMP concentrations on the Tafel polarization parameters for brass in 0.5 M HNO₃ at 25°C

[AMP] (mM)	E_{cor} (mV/SCE)	i_{cor} ($\mu\text{A cm}^{-2}$)	b_a (mV dec ⁻¹)	$-b_c$ (mV dec ⁻¹)	IE (%)	θ
0	- 61.41	51.50	48.28	221.61	/	/
0.5	- 65.94	24.30	55.35	204.08	52.81	0.5281
1	- 68.03	11.70	57.01	156.03	77.28	0.7728
5	- 91.35	06.20	60.78	134.10	87.79	0.8779
10	- 78.31	03.90	66.81	128.10	92.43	0.9243

To apprehend the complex process of the anodic dissolution of brass in a nitric acid medium, it is necessary to consider the dissolution of both metallic constituents of brass namely zinc and copper. Generally, the anodic reaction of copper consists of two successive steps [50,51]:



It should be noted that Cu⁺_{ads} ions are intermediate species which adsorb on the copper surface, they do not pass in solution. On the other hand, these monovalent ions oxidize to Cu²⁺, which will in turn reduce the alloy surface in the presence of Zn. However, their reduction is independent of the cathodic reaction of the system (60Cu-40Zn/ 0.5 M HNO₃). Zinc is the second important constituent of brass (60Cu-40Zn) and its anodic dissolution in nitric acid medium will occur according to the following reaction:



It is important to mention that this reaction takes place on different phases of the brass surface. Indeed, the (Cu-Zn) alloy is an (α , β') brass whose copper-rich alpha phase (59.5%) and zinc-rich beta phase (39.65%) are both susceptible to attack at different rates and therefore adsorption of the inhibitor will occur to different degrees on the two phases of the brass surface [52].

In a nitric acid environment, it is worth noting that the cathodic reaction is not a hydrogen gas evolution reaction at brass corrosion tests. Indeed, it is well known that the proton discharge reaction depends on the nature of the metal surface and that the hydrogen overpotential on brass is high, *i.e.* the corrosion potential of brass is higher than the equilibrium hydrogen evolution potential, in this acid solution. Therefore, corrosion of brass with hydrogen depolarization is thermodynamically highly improbable in nitric acid solution [53]. Consequently, the predominant cathodic process involves the reduction of nitrate ions which is accompanied by the dissolved oxygen reduction reaction in aerated acidic environments, according to the following reaction [50,54,55]:



In the solution containing free acid, nitrate ions are present and can easily reach the cathodic sites where reaction (4) occurs. On the other hand, in the solution with the inhibitor, AMP attaches to the active sites and forms a protective film on the surface of the brass. However, this film has defects that allow nitrate ions to diffuse through it, which are necessary for reaction (4) to occur on the bare surface. It is known that the diffusion of ions depends on their size, and the NO_3^- ion is larger than the Cu^{2+} and Zn^{2+} ions, making its diffusion slower and more difficult. Additionally, the presence of the adsorbed AMP molecules, with S, N, and O atoms, creates electronic repulsion against nitrate ions, further slowing down their reduction kinetics. When the inhibitor (AMP) is added to a 0.5 M HNO_3 acid solution, the rate of oxidation-reduction reactions at the brass electrode surface decreases, resulting in a noticeable decrease in cathodic and anodic current densities. The inhibitory efficiency values obtained using the polarization technique and gravimetric method are in good agreement.

3.2.2. Electrochemical impedance spectroscopy

In order to better understand the corrosion processes occurring at the interface between brass and the solution, the EIS technique was used. Nyquist and Bode plots of brass in a 0.5 M HNO_3 solution were obtained at various concentrations of AMP at 25°C, as shown in Figure 4.

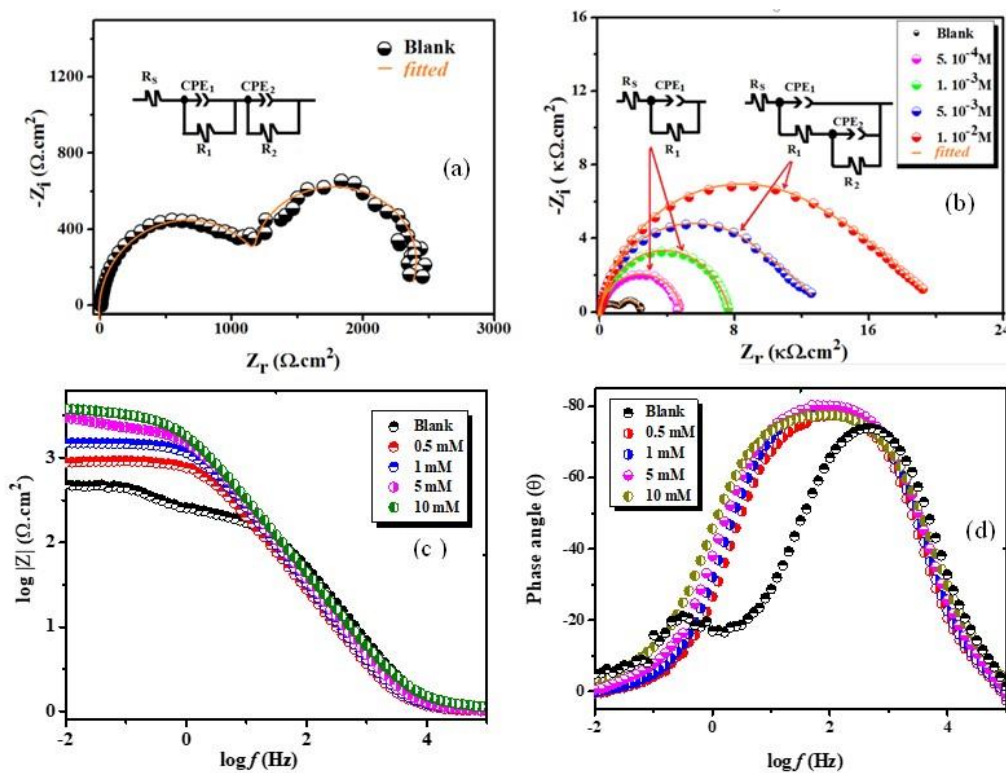


Figure 4. Effect of AMP on the Nyquist and Bode plots of brass corrosion in 0.5M HNO_3 at 25 °C

The impedance spectra were analyzed using suitable equivalent electrical circuits (Figure 4 inset), and the resulting data are presented in Table 3. It was observed that the appearance of the impedance diagrams for the 60Cu-40Zn alloy in the 0.5 M HNO₃ solution changed significantly in both shape and size when the AMP inhibitor was present. These changes were characterized by wider semi-circles compared to the blank solution (Figure 4a-b). Previous studies [56,57] have shown that the depressed semi-circles observed in the absence and presence of AMP are primarily caused by factors such as surface heterogeneity and roughness, dislocation, impurities, grain boundaries, adsorption-desorption of the inhibitor, and accumulation of species. Additionally, the enlargement of the diameter of the Nyquist diagrams in the presence of the inhibitor indicates significant adsorption of AMP on the brass surface, providing protection against the corrosive nature of the acid medium by blocking active sites [58]. Furthermore, the size of the diagrams increases as the concentration of the inhibitor increases, which suggests that a charge-transfer process primarily influences the corrosion of the alloy [59,60].

The Nyquist plot corresponding to the blank solution is represented by two distinct depressed semi-circles, located at the high and low frequency zones (Figure 4a). This observation is supported by the phase angle plot of the Bode diagram, where two well-defined time constants appeared (Figure 4b). Thus, an electrical equivalent circuit (EEC) corresponding to two-time constants in series, $R_s (R_1//CPE_1)$ and $(R_2//CPE_2)$ has been proposed to model the brass/0.5 M HNO₃ interface (Figure 4a. Inset). Accordingly, in this circuit, R_s represents the resistance of the electrolytic solution, the pair (R_1, CPE_1) is associated with the high-frequency domain, R_1 represents charge-transfer resistance with respect to the corrosion potential, and CPE_1 represents a constant-phase element that depicts a non-ideal double-layer capacitance. In the low frequencies range, the couple $(R_2//CPE_2)$ is characterized, R_2 represents the layer resistance formed by the corrosion products accumulated on the brass surface, and the constant phase element CPE_2 is related to the corrosion products layer. This latter is likely due to the redox phenomenon and adsorption species on the surface of the brass, it mainly consists of a copper deposit [56] and cuprous compounds such as $[Cu(NO_3^-)]_{ads}$ [61]. The effect of the different additions of AMP to acidic medium, on the impedance diagrams is highlighted in Figures 4b-d. The electrical equivalent circuits (EEC) modeling the (60Cu-40Zn) /solution interface, at different inhibitor concentrations, are shown in Figure 4b. As can be observed, when the inhibitor concentrations are at their lowest values (0.5 mM and 1 mM), the impedance diagrams show a depressed semi-circle with a single capacitive loop across the entire range of frequencies, which is characterized by the pair (R_1, CPE_1) . Therefore, the reason for the second half-circle being suppressed in relation to the blank solution is the adsorption of AMP molecules. These molecules create a barrier layer that protects the metal surface from acid attack. As a result, the formation of active galvanic couples and the buildup of corrosion products on the brass electrode surface are restricted. This interface has been properly modeled

by the circuit ($R_s (R_1 // CPE_1)$), inserted in Figure 4b. The impedance of the interfacial reaction between the inhibitor film and the bare metal is represented by the elements R_1 and CPE_1 . It is important to note that at higher inhibitor concentrations (5 and 10 mM), the impedance elongations at low frequencies in the complex reference frame clearly show the accumulation of species (such as water, ZnO, $[Cu(NO_3^-)]_{ads}$, etc.) at the interface. This corrosion products/solution interface is characterized by the resistance R_2 and the constant phase element CPE_2 .

The three EEC utilized for modeling the distinct interfaces, show a proper fit to the experimental data of the EIS diagrams with a minimal error and a chi-square value (χ^2) in order of 10^{-3} . In all the proposed electrical circuits, CPE was used to account for the non-ideality of the capacitance (C), resulting from roughness, surface heterogeneity, and the accumulation of species on the surface of metal which form a porous layer [62,63]. The CPE of the impedance is as follows [55,56,64]:

$$Z_{CPE} = Q^{-1} (j\omega)^{-n} \quad (15)$$

The CPE constant, denoted as Q , and the CPE exponent, denoted as n , indicate the heterogeneous nature of the surface. The angular frequency is represented by ω , and the imaginary number is $j^2 = -1$. After examining the impedance parameters in Table 3, it was observed that R_s did not show significant changes, even after the addition of AMP. However, the charge transfer resistance, R_1 , continuously and noticeably increased, while the double layer capacitance, C_1 , decreased while maintaining the same order of magnitude (a few $\mu F \text{ cm}^{-2}$). The capacitance was calculated using the following relationship [56,62]:

$$C = (Q R^{(1-n)})^{1/n} \quad (16)$$

The Helmholtz model states that the capacity (C) of the double layer is inversely proportional to the thickness (d) of the double layer, such that [53-55]:

$$C_{dl} = \frac{\varepsilon \varepsilon^0}{d} S \quad (17)$$

The surface of the electrode is represented by S , the permittivity of the air is represented by ε^0 , and the local dielectric constant is represented by ε . Therefore, based on Equation (17), the decrease in C_1 capacity can be attributed to either the decrease in the local dielectric constant of the aqueous medium, caused by the replacement of adsorbed water molecules with AMP molecules, or the increase in the thickness of the double layer. It is important to note that the thickening of the double layer is a result of the large number of AMP molecules adsorbed at the interface, forming a protective film that prevents the corrosive solution from affecting the brass surface. This finding is supported by the high values of activation resistance (R_1) obtained in the inhibitive solutions, indicating that the dissolution of brass was significantly slowed down by the expired drug.

Table 3. AMP influence on the EIS parameters of brass in 0.5 M HNO₃ at 25°C

[AMP] (mM)	0	0.5	1	5	10
R_S (Ω cm ²)	5.31	5.23	5.57	5.37	6.26
R_I (k Ω cm ²)	1.17	4.71	9.19	11.20	15.57
Q_1 (Ω^{-1} S ⁿ cm ⁻²) 10 ⁵	1.24	2.14	1.38	1.44	1.47
n_1	0.89	0.90	0.90	0.89	0.88
C_1 (μ F cm ⁻²)	7.35	6.55	4.03	3.65	3.23
R_2 (k Ω cm ²)	1.33	/	/	3.25	4.71
Q_2 (Ω^{-1} S ⁿ cm ⁻²) 10 ⁴	5.59	/	/	6.8	3.7
n_2	0.87	/	/	0.66	0.63
C_2 (μ F cm ⁻²)	183	/	/	1023	512.55
EI (%)	/	75.20	87.30	89.60	92.50
χ^2	0.003	0.001	0.001	0.002	0.003

Indeed, the inhibitory efficiency increased to the value of 92.50% at the maximal concentration of AMP (10 mM). It is important to note that even at the lowest concentration of 0.5 mM, there was still a significant inhibition efficiency of 75.20%.

The second time constant, which appeared when the inhibitor was present at high values, revealed several observations: (i) the resistance R_2 increased, but remained in the same order of magnitude as in the blank solution; (ii) the values of R_2 were significantly lower than those of R_I ; (iii) the capacitance C_2 increased, reaching values of a few hundred μ F cm⁻²; (iv) the values of the roughness factor n_2 were significantly lower than unity.

All these results indicate that the second semi-circle could be assigned to the formation of a porous film of corrosion products. This happens after the drug molecules have desorbed from the alloy surface, probably due to the metal dissolution [53].

The Bode diagrams shown in Figures 4c-d, reveal that the impedance modulus Z increased as the AMP amount increased at low frequencies. This suggests that the adsorption of the drug molecules enhanced the corrosion resistance of the brass in the aggressive solution [52,65]. Additionally, a shift in the phase angle towards more negative values and its enlargement in the presence of AMP confirmed that the drug strongly and efficiently adsorbed on the surface of the copper alloy in an acidic medium.

The corrosion inhibition efficacy of Ampicillin as a corrosion inhibitor for various metallic materials in aggressive solutions is summarized in Table 4 [66-70]. It is evident from this table that Ampicillin has not been previously used as a corrosion inhibitor for brass. The efficiency obtained in this study, using three different techniques, is very significant, exceeding 90%.

Table 4. Comparison of the inhibitory efficiency values of AMP reported in different studies with that obtained in this work

Inhibitor	Corrosive medium	Material	Inhibition Efficiency <i>EI</i> (%)			References
			Weight loss	Tafel	EIS	
AMP	1 M HCl	Carbon steel	/	97.7	95.5	[66]
AMP	0.5 M H ₂ SO ₄	Carbon steel	/	79.7	74.2	[66]
AMP	0.1 M H ₂ SO ₄	Mild steel	89.96	/	/	[67]
AMP + KBr	0.1 M H ₂ SO ₄	Mild steel	96.78	/	/	[67]
AMP + KCl	0.1 M H ₂ SO ₄	Mild steel	98.55	/	/	[67]
AMP + KI	0.1 M H ₂ SO ₄	Mild steel	95.37	/	/	[67]
AMP	2 M HCl	Aluminium	85.50	87.97	/	[68]
AMP	0.1 M H ₂ SO ₄	Mild steel	80.93	/	/	[69]
AMP	1 M HCl	Fe	91.80	95.79	95.83	[70]
AMP	0.5 M HNO ₃	Brass (Cu-40Zn)	91.17	92.43	92.50	This work

3.3. Temperature effect

Temperature is a factor that can affect both the behavior of metal in a corrosive environment and the nature of the interaction between the metal and inhibitor. In fact, an increase in temperature would cause the inhibitor to be released and organic compounds or complexes that have formed to dissolve quickly. This would result in a decrease in the metal's ability to resist corrosion. Data derived from the potentiodynamic polarization method were used to investigate the effect of temperature on the corrosion process of brass in the presence and absence of a drug. Table 5 presents the inhibitory efficiency (*EI* %) values and electrochemical parameters related to the corrosion of brass in 0.5 M HNO₃ before and after adding different concentrations of Ampicillin at temperatures ranging from 25 to 55 °C.

It is evident that increasing the temperature accelerates the corrosion rate in both the inhibited and uninhibited solutions, resulting in a decrease in inhibition efficiency. This could be attributed to the partial detachment of AMP molecules from the cathodic and anodic sites, leading to a moderate dissolution of the brass surface [71]. Notably, the inhibitor efficiency remains significant even at 55°C, as it maintains a high value of 80.23% at the optimal AMP concentration.

3.3.1. Arrhenius law

The investigation of the temperature effect during the corrosion study is very interesting because it allows us to evaluate the behavior of the brass corrosion and the stability of the

inhibiting layer. This evaluation also helps us to calculate the activation thermodynamic parameters related to the dissolution process of brass. Additionally, it provides more information on the type of inhibition mechanism by comparing the activation energy values before and after adding the inhibitor.

Table 5. Effect of temperature on the Tafel parameters for corrosion of brass in 0.5 M HNO₃ without and with different concentrations of AMP

<i>T</i> (°C)	[AMP] (mM)	<i>E</i> _{cor} (mV/SCE)	<i>i</i> _{cor} (μA cm ⁻²)	<i>b</i> (mV dec ⁻¹)	- <i>b</i> _c (mV dec ⁻¹)	<i>IE</i> (%)	θ
25	0	-61.41	51.50	48.28	221.61	/	/
	0.5	-65.94	24.30	55.35	204.08	52.81	0.5281
	1	-68.03	11.70	57.01	156.03	77.28	0.7728
	5	-91.35	06.20	60.78	134.10	87.79	0.8779
	10	-78.31	03.90	66.81	128.10	92.43	0.9243
35	0	-55.51	80.10	45.09	269.96	/	/
	0.5	-57.33	39.86	58.66	231.69	50.23	0.5023
	1	-84.38	20.90	64.33	154.62	73.90	0.7390
	5	-79.74	13.06	65.32	156.24	83.69	0.8369
	10	-79.42	08.73	68.34	161.48	89.10	0.8910
45	0	-66.10	117.42	57.06	290.77	/	/
	0.5	-76.60	62.22	79.24	171.69	47.01	0.4701
	1	-97.67	37.71	85.10	176.59	67.88	0.6788
	5	-77.82	24.40	70.66	170.90	79.21	0.7921
	10	-79.66	17.46	67.41	148.51	85.13	0.8513
55	0	-45.06	169.50	41.82	213.51	/	/
	0.5	-46.92	93.16	54.33	228.98	45.03	0.4503
	1	-76.37	65.52	87.37	217.40	61.34	0.6134
	5	-78.20	43.02	66.12	164.71	74.62	0.7462
	10	-78.61	33.50	74.39	163.60	80.23	0.8023

To determine the apparent activation energies (*E*_a) for the corrosion process, both with and without AMP at different concentrations in the acid solution, we used the Arrhenius formula [72]:

$$\ln i_{corr} = \ln A - \frac{E_a}{RT} \quad (18)$$

The corrosion current density is represented by *i*_{corr}, *A* represents the Arrhenius pre-exponential constant, *T* represents the absolute temperature, *R* represents the universal gas constant, and *E*_a represents the apparent activation energy. The plots of ln (*i*_{corr}) vs (1000/*T*) of brass in the absence and presence of various concentrations of inhibitor are displayed as straight lines over

the whole temperature range (not shown here), which indicates that the dissolution process of the brass has been described accurately by the Arrhenius kinetic law.

The purpose of studying of the temperature effect on corrosion inhibitors is to understand how these compounds adsorb on the metallic surface. To achieve this, we have focused on calculating the standard thermodynamic parameters, specifically the apparent energy E_a , the activation standard enthalpy ΔH_a° and the activation standard entropy ΔS_a° by studying the temperature function of the corrosion rate. In fact, an alternate relation of the Arrhenius transition state equation (19) enabled us to also compute ΔH_a° and the entropy ΔS_a° :

$$i_{\text{corr}} = \frac{RT}{Nh} \exp\left(\frac{\Delta S_a^\circ}{R}\right) - \exp\left(\frac{\Delta H_a^\circ}{RT}\right) \quad (19)$$

The Planck constant is represented by h , the Avogadro number is represented by N , the activation standard enthalpy is represented by ΔH_a° and the activation standard entropy is represented by ΔS_a° . Plots of $\ln(i_{\text{corr}}/T)$ vs $(1/T)$ are illustrated by straight lines (not shown here), whose slope is $(-\Delta H_a^\circ/R)$ and the intercept is $(\ln R/Nh + \Delta S_a^\circ/R)$, which permit the determination of ΔH_a° and ΔS_a° .

All the E_a and A pre-exponential factor values, 37.16, 48.05, 53.54, 59.44 (KJ mol⁻¹) and 7.91 10⁷, 2.99 10⁹, 1.51 10¹⁰, 1.02 10¹¹ (A cm⁻²), achieved in the presence of the inhibitor, are larger than without inhibitor, 32.84 KJ mol⁻¹ and 2.92 10⁷ A cm⁻², respectively, suggesting that the addition of AMP to the corrosive medium enhances the corrosion resistance of the brass [73,74].

Furthermore, the observed increase in activation energy when an inhibitor is present is often attributed to physical or electrostatic adsorption. In fact, as the temperature rises, there is a noticeable decrease in the inhibitor's adsorption on the metal surface [13,50]. The decrease in inhibitory efficiency as temperature increases can be explained by the shift of the adsorption-desorption equilibrium towards the desorption process. This leads to both the dissolution of brass and a decrease in the rate of the inhibitor's adsorption process. As a result, the surface coverage also decreases. This demonstrated that the formed adsorption film has a physical character [75]. In this study, it can be suggested that AMP is primarily adsorbed on the brass surface through physical interactions, as the inhibition efficiency does not decrease significantly with temperature. Specifically, at 55°C, the inhibition efficiency is 80.23%.

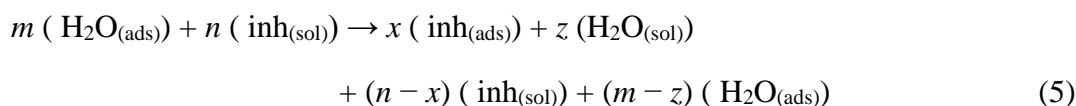
The positive sign of ΔH_a° indicates that the brass dissolution process is endothermic. In addition, the large values obtained of ΔH_a° in the presence of AMP, 34.56, 45.22, 50.85 and 56.75 KJ mol⁻¹ compared with that obtained in the acid alone (30.22 KJ mol⁻¹) suggest a slow corrosion of brass in the inhibitive solution [70]. Furthermore, the negative values of ΔS_a° ranged from -110.72 to -43.13 J mol⁻¹ K⁻¹ for the brass/HNO₃ system, indicate that the activated complex in the rate-determining step is an association rather than a dissociation. This implies that there is a decrease in disorder during the transformation of reactants into the activated complex [15,70]. Therefore, the degree of disorder on the brass surface decreases in the

presence of AMP, supporting the idea that a stable film of inhibitor is adsorbed on the brass surface, even at high temperatures. This is consistent with the inhibition efficiency determined at 55°C.

3.4. Adsorption isotherm and thermodynamic parameters

The main inhibition mode of organic inhibitors in electrolytic acid is related to their ability to form a protective layer on the metal surface [76].

The adsorption process of inhibitor molecules depends on their chemical structure, the distribution of charge in the molecules, the nature and surface charge of the metal, and the type and temperature of the aggressive medium [72]. By examining the chemical structure of the AMP molecule, we can see that its adsorption can occur through donor-acceptor interactions between π -electrons, N, O, and S heteroatoms of the inhibitor molecules, as well as the π -electrons of cationic species and the vacant d-orbital of copper and zinc [71]. The adsorption of AMP molecules at the brass-solution interface can be seen as a substitutional adsorption process between the inhibitive molecules in the aqueous solution ($\text{inh}_{(\text{sol})}$) and the water molecules on the metallic surface $\text{H}_2\text{O}_{(\text{ads})}$ [77]:



where (m) is the number of the adsorbed water molecules, (n) is the number of inhibitive molecules in solution, and (z) is the number of water molecules from the surface to the solution that were replaced by (x) inhibitor molecules from the solution to the surface.

To gain a better understanding of how brass corrosion is inhibited, we need to consider not only the direct adsorption of inhibitor molecules on the brass surface, but also the adsorption of inhibitor complexes like $(\text{Cu-inh})^{2+}$. These complexes are formed when inhibitor molecules combine with Cu^{2+} ions. Based on electrostatic attractions, the charged organo-metallic complexes are attracted and subsequently adsorbed onto the charged surface of the brass electrode [78]. Adsorption of other compounds such as $[\text{Cu}(\text{NO}_3^-) \text{inh}^+]_{\text{ads}}$ [61], and copper-like zinc complexes has also been reported [79,80]. Hence, such complex structures may beneficially contribute to the corrosion inhibition mechanism and improve the inhibitory properties of the adsorbed layer formed on the surface of brass [80].

In an attempt to identify the nature and potency of the adsorption of AMP molecules as a corrosion inhibitor, the potentiodynamic polarization experimental results (Table 5) were considered by adjusting the surface coverage (θ) values to diverse adsorption isotherms at various temperatures. The Langmuir adsorption isotherm can establish the closest correlation between the surface coverage degree (θ) and inhibitor AMP concentration (C_{inh}) in the nitric acid solution at all tested temperatures. Based on this isotherm (Eq. (20)) [81], (θ) is related to the inhibitor concentration C_{inh} , as below:

$$\frac{C_{inh}}{\theta} = \frac{1}{K_{ads}} + C_{inh} \quad (20)$$

The inhibitor concentration in the bulk solution is represented by C_{inh} , and the adsorption equilibrium constant of the adsorption process is represented by K_{ads} . Figure 5 shows the linear regressions between C_{inh}/θ and C_{inh} for each temperature within the concentration range of 0.5–10 mM.

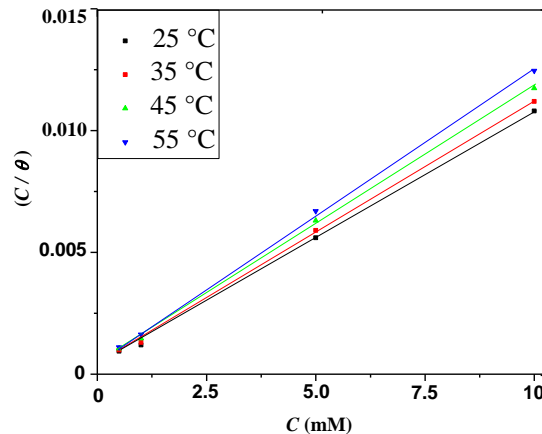


Figure 5. Langmuir adsorption isotherm plots for brass at different temperature

A perfectly linear plot was obtained with a correlation constant R^2 of 0.999 and a slope of around unity at all the temperatures, thereby validating this approach. The equilibrium constant, K_{ads} , the adsorption process is related to the standard free energy of adsorption (ΔG_{ads}°), also known as the standard Gibbs free energy, by this equation:

$$\Delta G_{ads}^\circ = -RT \ln(55.5 K_{ads}) \quad (21)$$

The universal gas constant, denoted as R , has a value of $8.3144 \text{ J K}^{-1}\text{mol}^{-1}$, T represents the thermodynamic temperature in Kelvin. The value 55.5 represents the concentration of water in the solution, expressed in mol per liter. The calculated values K_{ads} of adsorption process are $3.36 \cdot 10^3$, $2.78 \cdot 10^3$, $2.17 \cdot 10^3$ and $1.94 \cdot 10^3 \text{ M}^{-1}$ in the (25-55°C) range of temperature, respectively. As we can notice that, K_{ads} , referring to the adsorption capability of the inhibitor on the metallic surface, has large values, indicating that it is easily and strongly adsorbed onto the brass surface [82,83], which is consistent with the high inhibition performance of the tested inhibitor. Nevertheless, we note a decrease of K_{ads} as a function of temperature, but keeping the same magnitude, which suggests that the AMP molecules are partly desorbed from the surface.

The negative values of ΔG_{ads}° indicate that the inhibitor is spontaneously adsorbed onto the brass surface [84]. Generally, the energy values of -20 kJ mol^{-1} or less negative are assigned to an electrostatic interaction (physisorption) between charged molecules and charged metal surface; while those around -40 kJ mol^{-1} or more negative involves charge sharing or electron transfer from the inhibitor molecules to the metal surface, to form a coordinate covalent bond (chemisorptions) [55]. In the current study, the computed values of ΔG_{ads}° range between

-30.06 and -31.58 kJ mol⁻¹, which implies that the adsorption of the AMP molecules on the brass surface involves both physisorption and chemisorption at all temperatures. Indeed, the very negative values of ΔG_{ads}° exceed the physisorption domain and are close to that of chemisorption. The excellent inhibitory performance of AMP molecules can therefore be related to the presence of S and N atoms, in the molecular structure of the drug, which constitute the active adsorption sites [85].

Further explain the nature of adsorption, the experimental results were fitted into the Gibbs-Helmholtz equation (22) used to calculate the standard enthalpy of adsorption (ΔH_{ads}°) [76]:

$$\Delta G_{ads}^{\circ} = \Delta H_{ads}^{\circ} - T\Delta S_{ads}^{\circ} \quad (22)$$

The plot of ΔG_{ads}° vs T is illustrated by a straight line (not shown here); whose slope represents ΔS_{ads}° and the intercept is (ΔH_{ads}°). The negative values of ΔH_{ads}° indicate that adsorption of the AMP molecules onto the brass surface is an exothermic process [70].

Generally, an exothermic process will be indicative of physisorption, chemisorption or a mixture of the two processes [86]. For the physisorption, the value is rather less than -40 kJ mol⁻¹, whilst for chemisorption it is close to -100 kJ mol⁻¹ [87]. In the current study, the absolute value of ΔH_{ads}° for adsorption of AMP onto the brass surface is 15.45 kJ mol⁻¹, so it is lower than 40 kJ mol⁻¹ attesting that the physisorption phenomenon participates in to the process and becomes more dominant at elevated temperature [88]. On the other hand, the negative value of ΔS_{ads}° (-49.00 J mol⁻¹) is related to a decrease in disorder, as a result of desorption of water molecules from the metal surface. These last ones are replaced by inhibitor, which form an ordered adsorbed layer on the brass surface [77].

In light of the results obtained, namely: the thermodynamic parameters of activation and those of adsorption as well as the rather weak variation of the inhibition efficiency of AMP, as a function of the temperature, at the optimal concentration; it can be suggested that the mechanism of adsorption of AMP on the brass surface is a mixed type involving physical chemical interactions.

3.5. Surface morphology

3.5.1. SEM and EDX measurements

It is well known that microstructure factor is significant in the corrosion processes and inhibition of metallic corrosion. In this context, Figure 6 gives the SEM micrographs of the brass surface after polishing and after an immersion of 6H in without and with the optimal concentration of inhibitor (10 mM) in 0.5 M HNO₃ solution. The SEM image depicted in Figure 6a (inset) exhibits a smooth homogeneous surface with small fine scratches, resulting from mechanical polishing of the brass electrode. After plunging the brass into the aggressive solution for 6 hours, the micrograph of Figure 6b (inset) highlights that the surface is clearly attacked and damaged and that it is differentially corroded due to the presence of two phases,

one rich in copper (α) and the other rich in zinc (β'). Indeed, as copper is more noble than zinc, one can admit that the phase (α) forms the cathodic phase, which is the location of the reduction reaction of the solution and that the β' phase represents the anodic phase, which is the locus of the dissolution reaction of zinc. The evidence of a corroded brass surface is seen in the occurrence of cracks, pores or voids and the presence of corrosion products.

Contrarily, when an AMP inhibitor is present at its optimal concentration (10 mM), the Figure 6c (inset) clearly shows an improvement in the surface condition, the areas with defects have been repaired, cracks have been refilled and there are no signs of corrosion products are absent. Therefore, the presence of the AMP inhibitor results in a homogeneous and smooth surface, indicating the development of an organic protective layer on the electrode surface. This suggests that the corrosion of the brass has been significantly reduced.

Furthermore, the punctual EDX test was completed to identify the elemental composition of an area of the brass surface before and after 6 hours immersion in the absence and presence of the optimal concentration (10 mM) of AMP inhibitor.

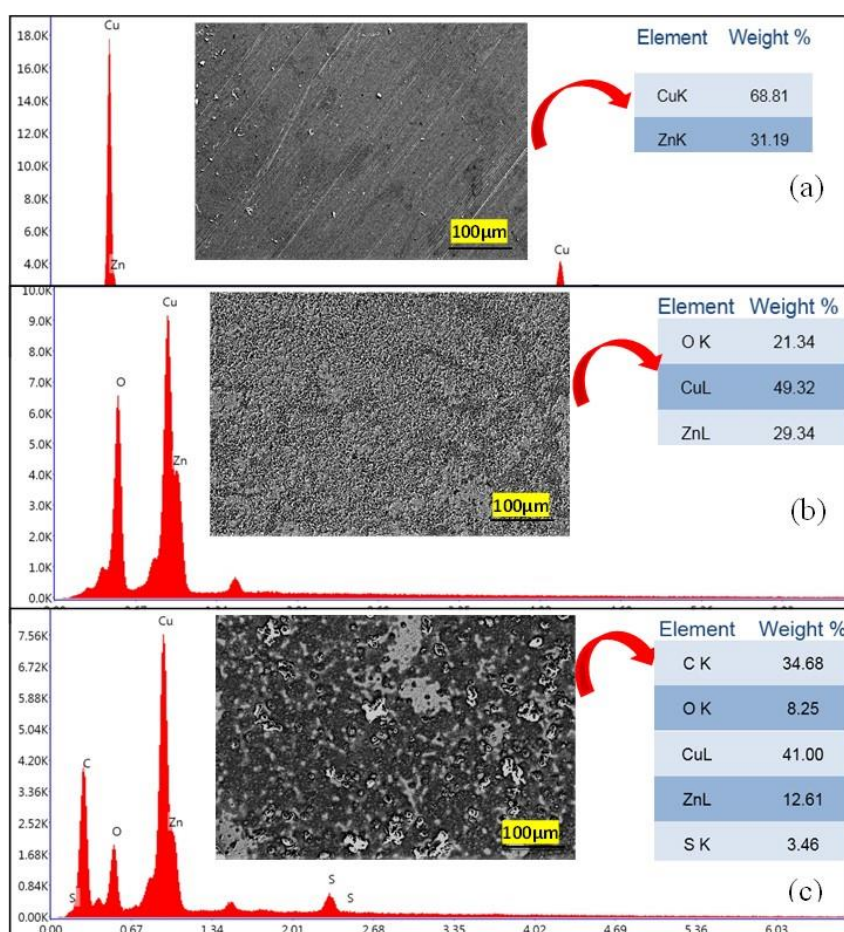


Figure 6. SEM micrographs associated with their EDX spectrums of brass samples a) As polished, b) immersed in 0.5M HNO₃ during six hours without inhibitor, and c) in the presence of 10⁻²M of AMP

The EDX pattern (Figure 6a) displays the typical peaks of the two main constituent elements, Cu and Zn, of the brass electrode utilized in the paper. After immersing the electrode in the aggressive solution (Figure 6b), exhibits an intense oxygen peak appeared, together with two peaks of Cu and Zn, which are less pronounced than the peaks of the un-corroded sample. These findings support the presence of metal oxides on the surface of the brass, which are corrosion products caused the dissolution of the Cu-alloy in the acid solution.

Meanwhile in the solution AMP inhibitor (Figure 6c), it was seen that the corresponding oxygen peak has been significantly diminished with the emergence of new C and S peaks thus confirming the adsorption of AMP molecules on the brass electrode surface which form a barrier layer, and with drawing the metal surface from the aggressiveness of the acidic solution tested.

3.5.2. FT-IR analysis

In order to ensure the successful adsorption of AMP on the brass surface, an FTIR analysis was conducted on both pure AMP and the film that was adsorbed on the brass surface [89]. The FT-IR spectrum of the adsorbed inhibitor film was compared to that of the expired drug (AMP). This comparison was done to confirm that AMP molecules were indeed adsorbed on the metal surface after being immersed in a 0.5 M nitric acid solution with 10 mM AMP for 6 hours. It was also done to identify the interaction sites between the inhibitor and the brass surface (Figure 7). Both spectra showed the same characteristic absorption bands that are typical of pure AMP. In the pure AMP spectrum, the bands at 1771, 1687, and 1494 cm^{-1} are assigned to the stretching of the aromatic ring and the vibrational stretching of the C-N bond. Additionally, the bands around 1020-1170 cm^{-1} and 588-696 cm^{-1} are due to the stretching of the aromatic ring and folding, respectively [16].

A broad peak with low intensity at 3444 cm^{-1} indicates the presence of a hydroxyl group, which is overlapped by the intense N-H stretching mode peak [90]. Aliphatic C-H stretching vibrations were observed at 2918 cm^{-1} , while aromatic C-H stretching vibrations were observed at 2969 cm^{-1} . The bands at 1687 cm^{-1} are attributed to the C=O stretching of the amide group. The absorption bands near 2969 cm^{-1} are attributed to the aromatic C-H stretching vibrations [66]. The weak peak at 1606 cm^{-1} in the pure AMP spectrum is attributed to N-H stretching. It is clear that almost all the peaks in the pure AMP spectrum are present in the spectrum of the film adsorbed on the brass surface.

This confirms that the protection of the brass surface against corrosion (Figure 7) is a result of the AMP molecules adsorbing onto its surface. However, we observed a shift in the bands and a change in the levels of adsorption in the spectrum of the adsorbed film compared to pure AMP. For instance, the C-N stretching bending band shifted by approximately 1420 cm^{-1} in the AMP film spectrum. The band at 1585 cm^{-1} is attributed to the N-H bending mode in the film spectrum, which is consistent with the data reported in the literature, specifically 1619.58 cm^{-1} for the AMP film on mild steel [67]. The band at 673 cm^{-1} was assigned to the Cu-N

stretching vibration, indicating that the inhibitor molecules interact with the brass surface and the N, O, and S hetero-atoms act as interaction centers. All of these findings demonstrate that the AMP molecules truly adsorbed onto the brass surface [16].

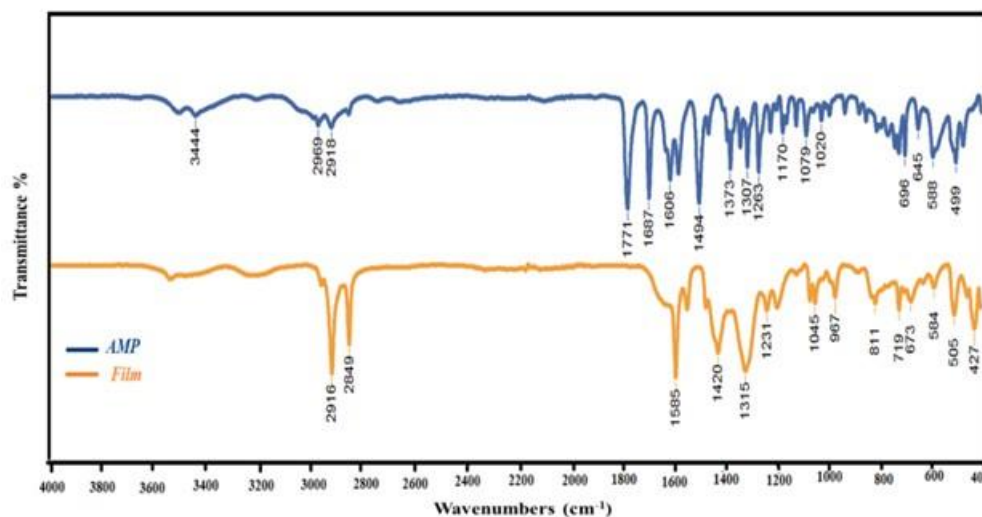


Figure 7. FT-IR spectra — pure AMP and — AMP film on the brass electrode

The used analysis techniques like SEM coupled with EDX and FT-IR allowed ascertaining the adsorption of AMP molecules on the surface of the brass electrode. Thus, in the presence of the AMP inhibitor in the corrosion tests, an inhibitive layer was formed on the brass surface with good stability and the existing pores are almost eliminated (lower permeability). As a result, the surface layer formed has good inhibiting properties and provides better protection of the brass electrode against corrosion in nitric acid solution.

3.6. Quantum chemical calculations

The experimental pre-selection of corrosion inhibitors can be very laborious, as it requires much time and laboratory equipment. The calculation of quantum descriptors is an excellent alternative to the experimental approach. Indeed, it enables to correlate the structure of the molecule with its reactivity, and therefore its adsorption and thus its effectiveness as a corrosion inhibitor. For these reasons, density functional theory (DFT) emerged as a highly valuable tool for analyzing experimental data and clarifying the corrosion inhibition mechanism [91]. The optimized structure of neutral and protonated Ampicillin is depicted in Figure 8. Meanwhile, the DFT parameters of the AMP molecule have been calculated and are listed in Table 6. The theory of frontier orbitals was useful in predicting the adsorption sites of the inhibitor molecule that interact with the atoms on the metallic surface [91].

The energy of the highest occupied molecular orbital (E_{HOMO}) tells us about the molecule's tendency to donate electrons. Therefore, higher E_{HOMO} values indicate a greater ability to

donate electrons, which improves the adsorption of the inhibitor onto the metal surface and increases its efficiency as an inhibitor. Additionally, the energy of the lowest unoccupied molecular orbital (E_{LUMO}) indicates the molecule's susceptibility to accepting electrons. Consequently, a lower E_{LUMO} value corresponds to higher inhibition efficiency.

Inspection of Figure 8 reveals that the HOMO orbitals of the neutral Ampicillin are primarily localized on the following hetero-atoms: S1, N2, O2, and O4, and to a lesser extent on the aromatic ring. While those of the protonated form are placed on O1 and N2 hetero-atoms, as well as on the aromatic ring. Concerning the LUMO orbitals of the neutral Ampicillin and that of the protonated form, they are localized only on the sulfur and carboxyl groups. It can therefore be deduced that the main active centers of the AMP molecule, which are the adsorption sites, are represented by the hetero-atoms.

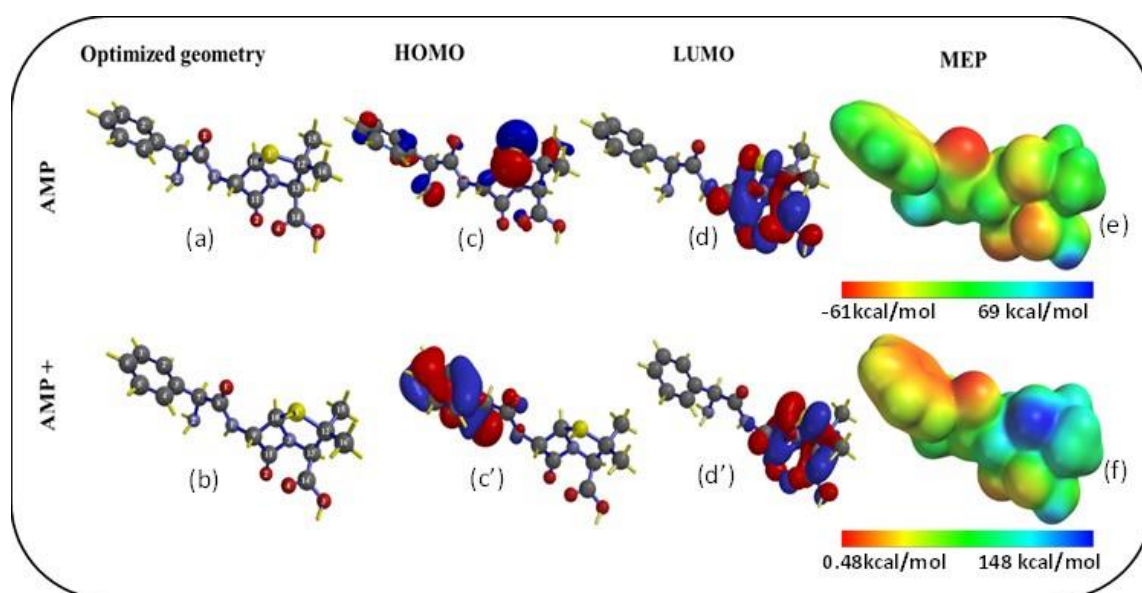


Figure 8. The optimized chemical structure of a) neutral and b) protonated AMP; topology of HOMO and LUMO orbitals for c), c') neutral and d), d') protonated AMP; molecular electrostatic potential (MEP) for e) neutral and f) protonated AMP

The quantum parameters in Table 6 show that when AMP is protonated, the E_{LUMO} value becomes more negative. This suggests that the protonated molecule has a stronger ability to accept electrons from brass atoms [92]. However, both the neutral and protonated forms of AMP have similar HOMO energy values, indicating that both can donate electrons to the empty orbitals of the metal atoms and form donor-acceptor coordinating bonds. Additionally, the energy gap (ΔE) of the protonated molecule is lower compared to that of the neutral molecule. This suggests that the protonated molecule has a stronger reactive power than the neutral molecule. It is widely reported in the literature that soft molecules are more reactive than hard molecules [93]. Indeed, the protonated AMP has the lowest value of the hardness (η), this means that it is softer, and hence more reactive than the neutral one.

Many studies [92,94] have considered the electrophilicity index (ω) of a molecule, which provides information on a molecule's ability to accept electrons. Indeed, the molecules with a small value of ω are more unlikely to accept electrons. In the view of certain authors [92,95], a molecule with a low electrophilicity index is a strong corrosion inhibitor. In this paper, AMP has the lowest value of ω , which means that the neutral form of AMP has a lower ability to accept electrons from the brass surface atoms. Therefore, it can be argued that the neutral inhibitor is more effective in preventing brass corrosion.

Table 6. Quantum chemical parameters for neutral and protonated AMP obtained using B3LYP/6-31G (d,p) in water phase

Inhibitor	E_{HOMO} (eV)	E_{LUMO} (eV)	ΔE (gap) (eV)	μ (Debye)	χ (eV)	η (eV)	ω (eV)	ε eV
AMP	-6.28	-0.50	5.78	7.43	3.39	2.89	1.98	0.5
AMP ⁺	-6.26	-1.37	4.89	14.05	3.81	2.44	2.97	0.34

Dipole moment (μ) values were also determined for AMP and AMP-H⁺; Both values are higher than that of water ($\mu_{H_2O} = 1.84$ Debye), which suggests that the inhibitor molecules have replaced the water molecules on the metal surface. Moreover, it is generally accepted that high (μ) values indicate of efficient inhibitor [96]. Based on the calculated DFT descriptors, it seems that both forms of AMP are likely to donate electrons to the brass surface providing efficient adsorption through donor-acceptor bonds.

The molecular electrostatic potential (MEP) shown in Figure 8, allows us to distinguish the location of electron density at different sites in the molecule.

These maps display various colors, with red indicating the negative potential area of the MEP, which is associated with reactive electrophilic sites. On the other hand, blue represents the positive area, which is the potential center for nucleophilic attacks [97].

In the case of neutral AMP, the red colored region is mainly focused on the N2, O2, and O4 hetero-atoms, while the blue region is located on the oxygen atom (O3). But for AMP-H⁺, the positive charge is clearly concentrated on the protonated sulfur atom (blue colored region) and as for the negative charge, it is localized on the oxygen (O1) and also on the benzene ring (red colored region).

As MEP surfaces have the inconvenient to supply information only on surface areas with high electron density and that with low electron density, the Fukui indices were then calculated. Indeed, the latter describe the atomic electron density changes resulting from the adding or removing of charges; they are more precise markers of which parts of the molecule are electrophilic or nucleophilic attacks. The computed Fukui indices, for both neutral and protonated AMP, are listed in Table 7.

In an attempt to find out which sites are most amenable to nucleophilic and electrophilic attacks, the Fukui indices f_k^+ and f_k^- , shown in Table 7, were calculated for both the neutral and protonated forms. They can also account for charge transfer by indicating the reactive centers of the molecule. Indeed, atoms with high f_k^+ are more prone to nucleophilic attack, whereas high f_k^- are more apt to be attacked by electron-deficient species [92,98,99].

Table 7. Calculated values of condensed Fukui indices for AMP and AMP⁺ by using B3LYP/6-31G (d,p) in water phase

AMP			AMP ⁺		
Atom	f^+	f^-	Atom	f^+	f^-
C1	0.016	0.033	C1	0.016	0.038
C2	0.009	0.074	C2	0.008	0.078
C3	0	0.049	C3	0.002	0.052
C4	0.022	0.076	C4	0.023	0.077
C5	0.014	0.023	C5	0.015	0.026
C6	0.008	0.094	C6	0.008	0.102
C7	0.017	0.009	C7	0.011	0.012
C8	0.019	0.039	C8	0.035	0.040
C9	0.010	0.010	C9	0.010	0.010
C10	0.029	0.010	C10	0.024	0.011
C11	0.105	0.028	C11	0.020	0.045
C12	0.017	1.002	C12	0.027	0.006
C13	0.004	0.003	C13	0.026	0.001
C14	0.098	0.004	C14	0.044	0.009
C15	0.007	0.006	C15	0.005	0.006
C16	0.027	0.004	C16	0.029	0.005
N1	0.011	0.010	N1	0.003	0.006
N2	0.010	0.103	N2	0.010	0.101
N3	0.057	0.003	N3	0.061	0.003
O1	0.015	0.054	O1	0.003	0.054
O2	0.122	0.024	O2	0.116	0.017
O3	0.050	0.003	O3	0.046	0.003
O4	0.103	0.009	O4	0.074	0.012
S1	0.087	0.029	S1	0.177	0.009

By analyzing the data in Table 7, it appears that the nucleophilic attack involves the most reactive sites, represented by the O2, O4 and C11 atoms for the neutral AMP and the O2 and S1 atoms for the protonated form. All these atoms are suitable to accept electrons from the brass surface. However, the C12 and N2 atoms for the neutral form and the C6 and N2 atoms for the protonated AMP, have the highest f_k^- values. This may indicate that electrons are being transferred to the empty orbitals of the metal surface in order to form coordinate bonds.

The results of the DFT study and of the local reactivity of the molecule allowed to determine all the reactive centers of the two forms of AMP, they corroborate those obtained by

the thermodynamic study. Indeed, the latter showed that AMP was able to adsorb, on the metal surface, by electrostatic and chemical bonds, which explains the high corrosion inhibition efficiency of brass by the expired drug in the acid solution.

3.7. Adsorption mechanism

On the basis of all the results gathered during this study, an adsorption mechanism can be suggested for brass/ HNO_3 + AMP system (Figure 9), to clarify the nature of inhibitor-brass interactions. The expired drug AMP has shown good ability to protect brass against corrosion in a nitric solution. The inhibitive effect of this drug is believed to be due to direct and/or indirect interactions between the drug molecules and the brass surface. The following factors are known to influence the adsorption process: the molecular structure, the molecular charge distribution, the charge of the metal surface, as well as the molecular protonation [16,72]. Given that in acidic solution, the two forms of AMP (neutral and protonated) are in equilibrium, two adsorption routes must be distinguished.

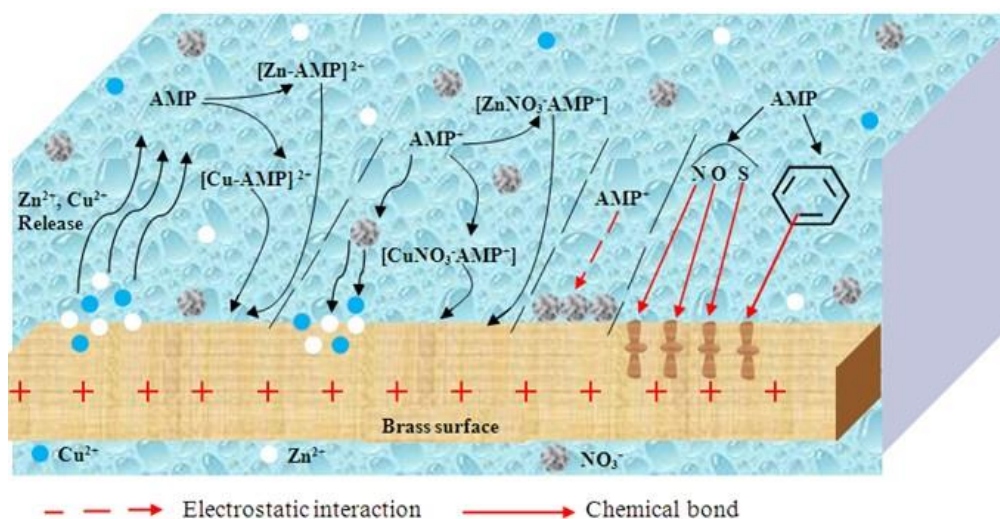


Figure 9. Simplified schema of the adsorption mechanism with the different interactions between AMP drug and brass surface

Indeed, after immersing the brass electrode in a nitric acid solution containing AMP, the π -electrons of the aromatic ring and the non-bonding pairs of the nitrogen, oxygen, and sulfur heteroatoms of the AMP molecules can interact with the empty d-orbitals of the copper and zinc atoms, based on electron transfer, this is a donor-acceptor type bond [71]. On the other hand, the protonated form (AMP-H^+) cannot directly adsorb onto the positively charged brass surface at the corrosion potential [16,64], thus the adsorption of nitrate ions (NO_3^-) on the brass surface charges this one negatively, thus supporting the adsorption of (AMP-H^+) by electrostatic attraction. Moreover, the interaction between neutral AMP and Cu^{2+} ions, emerging from the metal surface, leads to the formation of the $[\text{Cu-AMP}]^{2+}$ complex and to its

adsorption on the brass surface by coordinate bonds [78]. The adsorption of other complexes such as $[\text{Cu}(\text{NO}_3)_2\text{AMP}]_{\text{ads}}^+$ must be considered [61]. It is noteworthy that zinc can form complexes with a structure that is similar to that of copper [79,80]. These findings emphasize the conjoint contribution of AMP molecules, AMP- H^+ molecules and different complexes to the corrosion inhibition mode and thereby to the protection of brass alloy against attack by the nitric acid solution.

4. CONCLUSION

A short This work deals with a novel study of expired Ampicillin (AMP) as a corrosion inhibitor for brass in nitric acid electrolyte at various concentrations.

The gravimetric tests showed that the corrosion rate (CR) increased as the concentration of the nitric acid blank solution increased, in the presence of AMP; it decreased, resulting in an inhibition efficiency of over 91% at the optimal concentration of 10 mM, regardless of the acid concentration. Furthermore, it was observed that the inhibition efficiency increased as the acid concentration increased, reaching a value of 95.36% in the 2 M HNO_3 solution. Based on the polarization curves, it was determined that AMP acts as a mixed inhibitor and does not change the mechanism of nitrate reduction in a 0.5 M HNO_3 solution. In the EIS study, the resistance of the charge transfer value increased as the concentration of AMP was raised, which suggests that the brass dissolved weakly in the presence of the drug. The large negative values of ΔG_{ads}^0 confirmed the spontaneous and combined adsorption mode, in which physical and chemical interactions are involved in the global adsorption process of AMP on the brass surface. Such adsorption was confirmed by SEM coupled with EDX and FT-IR analysis. Quantum chemical calculations were used to identify the atomic sites likely to be involved in the interactions between the inhibitor and the surface of brass. Indeed, all the active centers of the AMP were determined by means of DFT and Fukui indices, which define the electrophilic and nucleophilic sites in the molecule. It can be concluded that the theoretical results are reasonably consistent with the results obtained from both electrochemical and thermodynamic studies. These studies have shown that AMP is an effective corrosion inhibitor for brass in a 0.5 M HNO_3 solution.

Declarations of interest

The authors declare no conflict of interest in this reported work.

REFERENCES

- [1] S. Hosseinpour, M. Forslund, C.M. Johnson, J. Pan, and C. Leygraf, Surf. Sci. 648 (2016) 70.
- [2] D. Özkir, E. Bayol, A.A. Gürten, Y. Sümme, and F. Kandemirli, Chem. Pap. 67 (2013)

- 202.
- [3] R. Gasparac, C.R. Martin, and E. Stupnisek-Lisac, *J. Electrochem. Soc.* 147 (2000) 548.
- [4] M. Abdallah, M.A. Agez, and A.S. Fouda, *Int. J. Electrochem. Sci.* 4 (2009) 336.
- [5] K.F. Khaled, *Corros. Sci.* 52 (2010) 3225.
- [6] S. Selvaraj, S. Ponmariappan, M. Natesan and N. Palaniswamy, *Corros. Rev.* 21 (2003) 41.
- [7] P. Zhou, M.J. Hutchison, W. Erning, J.R. Scully, and K. Ogle, *Electrochim. Acta* 229 (2017) 141.
- [8] A.G. Gad-Allah, M.M. Abou-Romia, M.W. Badawy, and H.H. Rehan, *J. Appl. Electrochem.* 21 (1991) 829.
- [9] T. Zhang, W. Jiang, W.H. Wang, and S. Zhang, *J. Adhes. Sci. Technol.* 34 (2019) 25.
- [10] S.J. Gregg, and K.S.W. Singh, *Adsorption surface area and porosity*, Academic Press, London (1967) 19.
- [11] O.L. Riggs, *Corrosion Inhibitors*, in C.C. Nathan (Ed), NACE (1973) 7.
- [12] C.A. Loto, and R.T. Lot, *Silicon* 10 (2018) 2877.
- [13] M. Mihit, S. El Issami, M. Bouklah, L. Bazzi, B. Hammouti, E. Ait Addi, R. Salghi, and S. Kertit, *Appl. Surf. Sci.* 252 (2006) 2389.
- [14] A.K. Singh, A.K. Pandey, P. Banerjee, S.K. Saha, B. Chugh, S. Thakur, B. Pani, P. Chaubey, and G. Singh, *J. Environ. Chem. Eng.* 7 (2019) 102971.
- [15] R.T. Vashi, *Int Res. Appl. Sci. Eng. Technol.* 8 (2020) 2124.
- [16] A. El-asri, A. Jmiai, Y. Lin, A. Taoufouq, M.M. Rguiti, H. Bourzi, and S. El Issami, *Int. J. Corros. Eng. Sci. Technol.* 57 (2022) 680.
- [17] S. Mo, H.Q. Luo, and N.B. Li, *J. Colloid Interface Sci.* 505 (2017) 929.
- [18] Ž.Z. Tasić, M.B. Petrović Mihajlović, M.B. Radovanović, A.T. Simonović, and M.M. Antonijević, *J. Mol. Struct.* 1159 (2018) 46.
- [19] J. Li, D. Chen, D. Zhang, Y. Wang, Y. Yu, L. Gao, and M. Huang, *Colloids Surf., A* 550 (2018) 145.
- [20] Z. Ghelichkhal, S. Sharifi-Asl, K. Farhadi, S. Banisaied, S. Ahmadi, and D.D. Macdonald, *Corros. Sci.* 91 (2015) 129.
- [21] D. Wang, B. Xiang, Y. Liang, S. Song, and C. Liu, *Corros. Sci.* 85 (2014) 77.
- [22] M. Finšgar, and D. Kek Merl, *Corros. Sci.* 83 (2014) 164.
- [23] X. Zheng, S. Zhang, W. Li, L. Yin, J. He, and J. Wu, *Corros. Sci.* 80 (2014) 383.
- [24] J. Chen, Z. Qin, T. Martino, and D.W. Shoesmith, *Corros. Sci.* 114 (2017) 72.
- [25] H.J. Yu, C.X. Li, B.Y. Yuan, L. Li, and C. Wang, *Corros. Sci.* 120 (2017) 231.
- [26] Y. Zhou, L. Guo, Z.H. Zhao, S.S. Zheng, Y. Xu, B. Xiang, and S. Kaya, *J. Adhes. Sci. Technol.* 32 (2018) 1485.
- [27] C. Verma, E.E. Ebenso, I. Bahadur, and M.A. Quraishi, *J. Mol. Liq.* (2018) 577.
- [28] N. Kovacevic, I. Milosev, and A. Kokalj, *Corros. Sci.* 124 (2017) 25.

- [29] A. Belafhaili, M. El Hawary, A. Bellaouchou, A. Guenbour, I. Warad, and A. Zarrouk, *Anal. Bioanal. Electrochem.* 15 (2023) 118.
- [30] M. Li, J. Xu, R. Li, D. Wang, T. Li, M. Yuan, and J. Wang, *J. Colloid Interface Sci.* 417 (2014) 131.
- [31] Y. Qiang, S. Zhang, S. Yan, X. Zou, and S. Chen, *Corros. Sci.* 126 (2017) 295.
- [32] M. Finšgar, *Corros. Sci.* 72 (2013) 82.
- [33] I. Lozano, E. Mazario, C.O. Olivares-Xometl, N.V. Likhanova, and P. Herrasti, *Mater. Chem. Phys.* 147 (2014) 191.
- [34] V.V. Mehmeti, and A.R. Berisha, *Front. Chem.* 5 (2017) 61.
- [35] K.S. Bokati, C. Dehghanian, and S. Yari, *Corros. Sci.* 126 (2017) 272.
- [36] X. Zheng, S. Zhang, W. Li, M. Gong, and L. Yin, *Corros. Sci.* 95 (2015) 168.
- [37] L. Guo, S. Kaya, I.B. Obot, X. Zheng, and Y. Qiang, *J. Colloid Interface Sci.* 506 (2017) 478.
- [38] L.B. Coelho, M. Mouanga, M.E. Druart, I. Recloux, D. Cossement, and M.G.A.S. Olivier, *Corros. Sci.* 110 (2016) 143.
- [39] G. Gece, *Corros. Sci.* 53 (2011) 3873.
- [40] M. Metikos-Hukovic, R. Babic, and I. Paic, *J. Appl. Electrochem.* 30 (2000) 617.
- [41] M. Mashuga, L. Olasunkanmi, A. Adekunle, S. Yesudass, M. Kabanda, and E. Ebenso, *Mater.* 8 (2015) 3607.
- [42] W. Li, J. Landon, B. Irvin, L.F. Zheng, K. Ruh, L. Kong, J. Pelgen, D. Link, J.D. Figueroa, J. Thompson, H. Nikolic, and K. Liu, *Ind. Eng. Chem. Res.* 56 (2017) 4792.
- [43] P.B. Mathur, and T. Vasudevan, *Corros.* 38 (1982) 171.
- [44] X. Wang, H. Yang, and F. Wang, *Corros. Sci.* 53 (2011) 113.
- [45] S. Deng, X. Li, and H. Fu, *Corros. Sci.* 53 (2011) 760.
- [46] S. Deng, and X. Li, *Corros. Sci.* 55 (2012) 407.
- [47] G. Sigircik, D. Yildirim, and T. Tuken, *Corros. Sci.* 120 (2017) 184.
- [48] Y. Qiang, S. Zhang, S. Xu, and L. Yin, *RSC. Adv.* 5 (2015) 63866.
- [49] Z. Hu, Y. Meng, X. Ma, H. Zhu, J. Li, C. Li, and D. Cao, *Corros. Sci.* 112 (2016) 563.
- [50] X. Zang, W.F. Jiang, H.L. Wang and C. Hao, *J. Adhes. Sci. Technol.* 33 (2019) 1.
- [51] R. Solmaz, E.A. Şahin, A. Döner, and G. Kardaş, *Corros. Sci.* 53 (2011) 3231.
- [52] H. Gerengi, K. Schaefer, and H.I. Sahin, *J. Ind. Eng. Chem.* 18 (2012) 2204.
- [53] I.K. Marshakov, *Protec. Met.* 41 (2005) 205.
- [54] K.F. Khaled, *Corros. Sci.* 52 (2010) 3225.
- [55] M. Ebrahimzadeha, M. Gholamia, M. Momenia, A. Kosaria, M.H. Moayeda, and A. Davoodib, *Appl. Surf. Sci.* 332 (2015) 384.
- [56] I. Rotaru, S. Varvara, L. Gaina, and L.M. Muresan, *Appl. Surf. Sci.* 321 (2014) 188.
- [57] H.O. Curkovic, E. Stupnisek-Lisac, and H. Takenouti, *Corros. Sci.* 51 (2009) 2342.

- [58] K. Mansikkamaki, U. Haapanen, C. Johans, K. Koutturi, and M. Valden, *J. Electrochem. Soc.* 153 (2006) B311.
- [59] K.C. Emregul, and O. Aakol, *Mater. Chem. Phys.* 82 (2003) 188.
- [60] H. Fan, S. Li, Z. Zhao, H. Wang, Z. Shi, and L. Zhang, *Corros. Sci.* 53 (2011) 4273.
- [61] P. Hu, Z. Wu, J. Wang, Y. Huang, Q. Liu, S. Zhou, *Green Energy Environ.* 5 (2020) 214.
- [62] R. Fuchs-Godec, *J. Mol. Liq.* 228 (2016).
- [63] F. Suedile, F. Robert, C. Roos, and M. Lebrini, *Electrochim. Acta* 133 (2014) 631.
- [64] J. Jennane, M.E. Touhami, S. Zehra, Y. Baymou, S.H. Kim, I.M. Chung, and H. Lgaz, *Mater. Chem. Phys.* 227 (2019) 200.
- [65] R.J.L. Welbourn, C.L. Truscott, M.W.A. Skoda, A. Zorbakhsh, and S.M. Clarke, *Corros. Sci.* 115 (2017) 68.
- [66] G. Golestani, M. Shahidi, and D. Ghazanfari, *Appl. Surf. Sci.* 308 (2014) 347.
- [67] N.O. Eddy, E.E. Ebenso, and U.J. Ibok, *J. Appl. Electrochem.* 40 (2010) 445.
- [68] M. Abdallah, *Corros. Sci.* 46 (2004) 1981.
- [69] N.O. Eddy, U.J. Ibok, E.E. Ebenso, A. El Nemr, and El Sayed H. El Ashry, *J. Mol. Model.* 15 (2009) 1085.
- [70] M. Abdallah, A. Al Bahir, H.M. Altass, A. Fawzy, N. El Guesmi, Arej S. Al-Gorair, F. Benhiba, I. Warad, and A. Zarrouk, *J. Mol. Liq.* 330 (2021) 115702.
- [71] J.R. Xavier, and R. Nallaiyan, *J. Solid. State Electrochem.* 16 (2012) 391.
- [72] J. Aljourani, K. Raeissi, and M.A. Golozar, *Corros. Sci.* 51 (2009) 1836.
- [73] M.K. Pavithra, T.V. Venkatesha, M.K. Punith Kumar, and N.S. Anantha, *Res. Chem. Intermed.* 42 (2016) 2409.
- [74] N. Raghavendra, and J. Ishwara Bhat, *Res. Chem. Intermed.* 42 (2016).
- [75] M. Lebrini, F. Robert, A. Lecante, and C. Roos, *Corros. Sci.* 53 (2011) 687.
- [76] E.A. Noor, *Int. J. Electrochem. Sci.* 2 (2007) 996.
- [77] M. Slimane, F. Kellou, and S. Kellou-Tairi, *Res. Chem. Intermed.* 41 (2015) 8571.
- [78] S. Martinez, and I. Stern, *J. Appl. Electrochem.* 31 (2001) 973.
- [79] G. Gao, and C.H. Liang, *Corros. Sci.* 49 (2007) 3479.
- [80] H. Gerengi, K. Schaefer, and H.I. Sahin, *J. Ind. Eng. Chem.* 18 (2012) 2204.
- [81] D. Ozkır, K. Kayakırılmaz, E. Bayol, A. Ali Gurten, and F. Kandemirli, *Corros. Sci.* 56 (2012) 143.
- [82] X. Li, S. Deng, H. Fu, and T. Li, *Electrochim. Acta* 54 (2009) 4089.
- [83] N. Djeddi, M. Benahmed, S. Akkal, H. Laouer, E. Makhloufi, and N. Gherraf, *Res. Chem. Intermed.* 41 (2015) 4595.
- [84] I. Ahamad, R. Prasad, and M.A. Quraishi, *Corros. Sci.* 52 (2010) 1472.
- [85] F. Bentiss, M. Lebrini, and M. Lagrenee, *Corros. Sci.* 47 (2005) 2915.
- [86] Y. Abboud, A. Abourriche, T. Saffaj, M. Berrada, M. Charrouf, A. Bennamara, and H. Hannache, *Desalination* 237 (2009) 175.

- [87] E.A. Noor, and A.H. Al-Moubaraki, *Mater. Chem. Phys.* 110 (2008) 145.
- [88] X. Li, S. Deng, and H. Fu, *Corros. Sci.* 62 (2012) 163.
- [89] A. Lalitha, S. Ramesh, and S. Rajeswari, *Electrochim. Acta* 51 (2005) 47.
- [90] I.B. Obot, and A. Madhankumar, *Mater. Chem. Phys.* 177 (2016) 266.
- [91] S. Martinez, and I. Stagljar, *J. Mol. Struct. Theochem.* 640 (2003)167.
- [92] M.R.N. El-Din, and E.A. Khamis, *J. Surfact. Deterg.* 17 (2014) 795.
- [93] L. Madkour, S. Kaya, C. Kaya, and L. Guo, *J. Taiwan Inst. Chem. E* 68 (2016) 461.
- [94] R. G. Parr, L. Szentpaly, and S. Liu, *J. Am. Chem. Soc.* 121 (1999) 1922.
- [95] W. Huang, Y. Tan, B. Chen, J. Dong, and X. Wang, *Tribol. Int.* 36 (2003) 163.
- [96] N.O. Eddy, and I.I. Benedict, *J. Mol. Mod.* 7 (2011) 359.
- [97] A.M. Al-Sabagh, N.M. Nasser, A.A. Farag, M.A. Migahed, A.M.F. Eissa, and T. Mahmoud, *Egypt J. Pet.* 22 (2013) 101.
- [98] I. B. Obot, S. Kaya, C. Kaya, and B. Tuzun, *Res. Chem. Intermed.* 42 (2016) 4963.
- [99] M.A. Hegazy, *J. Mol. Liq.* 208 (2015) 227.